processes

MDPI

Article

Paleoenvironmental Conditions and Shale Oil Potential of the Carboniferous Ha'erjiawu Formation in the Santanghu Basin, NW China

Shaohua Zhang [1,*], Chiyang Liu [2], Zhiqiang Fan [3,*], Hao Liang [4], Jianrong Gao [5], Hui Song [5], Wei Dang [1], Long Zhang [1] and Yaning Gao [1]

[1] Shaanxi Key Laboratory of Petroleum Accumulation Geology, School of Earth Sciences and Engineering, Xi'an Shiyou University, Xi'an 710065, China; longzh1225@126.com (L.Z.)
[2] State Key Laboratory of Continental Dynamics, Department of Geology, Northwest University, Xi'an 710069, China
[3] No. 2 Gas Production Plant, Petro-China Changqing Oilfield Company, Xi'an 710200, China
[4] Petro-China Turpan-Hami Oilfield Company, Hami 839009, China; lianghao@petrochina.com.cn
[5] Research Institute of Petroleum Exploration and Development, Petro-China, Beijing 100083, China; gaojianrong@petrochina.com.cn (J.G.)
* Correspondence: zhangshh@xsyu.edu.cn (S.Z.); fanzhiqiang2@petrochina.com.cn (Z.F.)

Abstract: The Carboniferous Ha'erjiawu Formation in the Santanghu Basin represents a significant potential target for shale oil exploration, yet its characteristics remain largely unknown. This study utilizes a combination of elemental and organic geochemical analyses to investigate the paleoenvironmental conditions and shale oil potential of the Carboniferous Ha'erjiawu Formation black shales within the Santanghu Basin. The results suggest that the Ha'erjiawu Formation black shales were deposited in water columns with low salinity and dysoxic conditions, as indicated by paleosalinity and redox proxies such as Rb/K, B/Ga, B content, V/Cr, V/(V + Ni), V/Al, and Mo/Al. Furthermore, the climatic proxies (Ga/Rb, Sr/Cu and K_2O/Al_2O_3) indicate that the Santanghu Basin underwent a warm-humid/cold-dry oscillating climate during the deposition of the Ha'erjiawu Formation black shales, potentially influenced by synsedimentary volcanic activity or the Late Paleozoic glaciation. The organic geochemical analyses have revealed that the Ha'erjiawu Formation black shales are rich in type II kerogen, which is in the early mature to mature stage, indicating a significant potential for oil generation. However, there is considerable variation in the oil content of the analyzed samples, with only a few containing movable oil. Given the high abundance of brittle minerals within the Ha'erjiawu Formation black shales, it will be indispensable to meticulously evaluate and identify intervals exhibiting abundant movable oil for successful shale oil exploration and development within this geological unit.

Keywords: paleoenvironmental conditions; shale oil; black shale; Ha'erjiawu Formation; Santanghu Basin

check for updates

Citation: Zhang, S.; Liu, C.; Fan, Z.; Liang, H.; Gao, J.; Song, H.; Dang, W.; Zhang, L.; Gao, Y. Paleoenvironmental Conditions and Shale Oil Potential of the Carboniferous Ha'erjiawu Formation in the Santanghu Basin, NW China. *Processes* **2023**, *11*, 2209. https://doi.org/10.3390/pr11072209

Academic Editors: Jianhua Zhao, Guoheng Liu, Xiaolong Sun and Yuqi Wu

Received: 13 May 2023
Revised: 17 July 2023
Accepted: 18 July 2023
Published: 22 July 2023

1. Introduction

With the depletion of conventional hydrocarbon resources and the advancement in theoretical innovations for hydrocarbon exploration, shale oil resources within source rocks have garnered significant attention from researchers and explorers over the past few decades [1–5]. With the aid of technological advancements, such as horizontal drilling and hydraulic fracturing, the United States has taken a leading role in commercializing shale oil production, which has become the primary catalyst for crude oil output growth within its borders [2,6]. Inspired by the successful development of shale oil in the United States, China has conducted extensive exploration and research on shale oil over the past decade [3,7,8]. Currently, several commercially exploitable shale oil plays have been found in several basins in China [8], such as the Cretaceous Qingshankou Formation in the

Songliao Basin [9,10], the Paleogene Shahejie Formation in the Bohai Bay Basin [11,12], the Paleogene Qianjiang Formation in the Jianghan Basin [13,14], the Triassic Yanchang Formation in the Ordos Basin [15,16], the Jurassic System in the Sichuan Basin [17,18], the Permian Fengcheng and Lucaogou Formations in the Junggar Basin [19,20] and the Permian Lucaogou Formation in the Santanghu Basin [21–23]. It is noteworthy that China's shale oil resources are primarily situated in lacustrine basins, which typically exhibit greater heterogeneity than North American marine shale [6]. This heterogeneity results in generally low well productivity in Chinese shale oil exploration, and an extremely uneven distribution of high- and low-yield wells [6,8]. The heterogeneity of lacustrine shale is primarily influenced by paleoenvironmental conditions; thus, a thorough investigation into the paleoenvironment of lacustrine shale is imperative for precise estimation of its potential as a source of shale oil.

The Santanghu Basin boasts abundant conventional and unconventional hydrocarbon resources, thanks to the presence of multiple layers of black shales [24,25]. Among these black shales, the Permian Lucaogou Formation black shales have been proven to be a commercially viable shale oil play [21–23,25]. Whether other shales possess commercially viable shale oil resources, particularly the Carboniferous Ha'erjiawu Formation with geological conditions comparable to the Lucaogou Formation [24,26], remains a pressing issue in the exploration of shale oil within the Santanghu Basin. Due to the divergent opinions regarding whether the Carboniferous paleogeographic environment of the Santanghu Basin was an epicontinental sea-lagoon or lake, the paleoenvironmental conditions of the Ha'erjiawu Formation black shales remain ambiguous, impeding accurate assessment of shale oil resources [24,26]. The paleoenvironmental conditions of shale are intimately linked to the quantity and quality of organic matter, which is a pivotal factor in assessing the potential for shale oil exploration [1,3,6]. Elemental geochemistry has proven to be a valuable tool in reconstructing paleoenvironmental conditions of shale [9,16,22]. Therefore, this study integrates elemental and organic geochemistry data to constrain the paleoenvironmental conditions of the Carboniferous Ha'erjiawu Formation black shale in the Santanghu Basin, and provides a preliminary assessment of its shale oil exploration potential.

2. Geological Setting

The Santanghu Basin, located in northwest China, is a petroleum-rich basin surrounded by the Junggar Basin to the west, the Turpan-Hami Basin to the south, and the Republic of Mongolia to the northeast (Figure 1a). Tectonically, the Santanghu Basin, trending NW–SE and sandwiched between the Kalameili and Aermantai ophiolite belts, is a typical intramontane basin with a multicycle evolutionary history [21,22]. It is widely accepted that the Santanghu region underwent the following evolutionary stages subsequent to oceanic basin closure: (1) regional extension and rifting from the Late Carboniferous to the Middle Permian; (2) tectonic contraction and inversion during the Middle Permian-Early Triassic; (3) continuous thermal subsidence from the Middle Triassic to Early Cretaceous, punctuated by two short episodes of tectonic uplift in Late Triassic and Late Jurassic; (4) tectonic inversion and uplifting during the Late Cretaceous; and (5) regional wrench faulting and basin reformation during the Cenozoic [22].

The Santanghu Basin comprises three substructural units, namely, the Southwest Fold-and-Thrust Belt, Central Depression Belt, and Northeast Fold-and-Thrust Belt (Figure 1b). The residual sedimentary strata are predominantly preserved within the Central Depression Belt, exhibiting a maximum thickness of 6500 m [27]. The Carboniferous strata, comprising the Donggulubasitao Formation, Jiangbasitao Formation, Bashan Formation, Ha'erjiawu Formation, and Kalagang Formation in ascending order (Figure 2), are interpreted as having been deposited in a neritic or marine-terrigenous alternating environment accompanied by volcanism [24,26]. The Ha'erjiawu Formation, which is the focus of this study, primarily consists of basalt, andesite, tuff, tuffaceous sandstone, tuffaceous shale, and carbonaceous shale. Research conducted over the past decade has demonstrated that the tuffaceous shale and carbonaceous shale within the Ha'erjiawu Formation are abundant in organic matter, and represent a significant source rock within the Santanghu Basin [24,26].

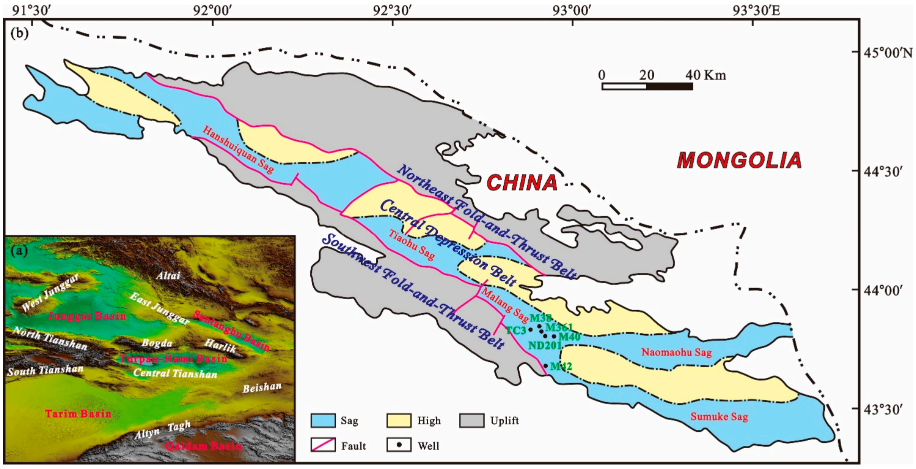

Figure 1. (**a**) DEM image of Northwest China and adjacent area with major basins and mountains labeled; (**b**) tectonic sketch map showing the major structural elements of the Santanghu Basin with the location of sampled drilled wells labeled.

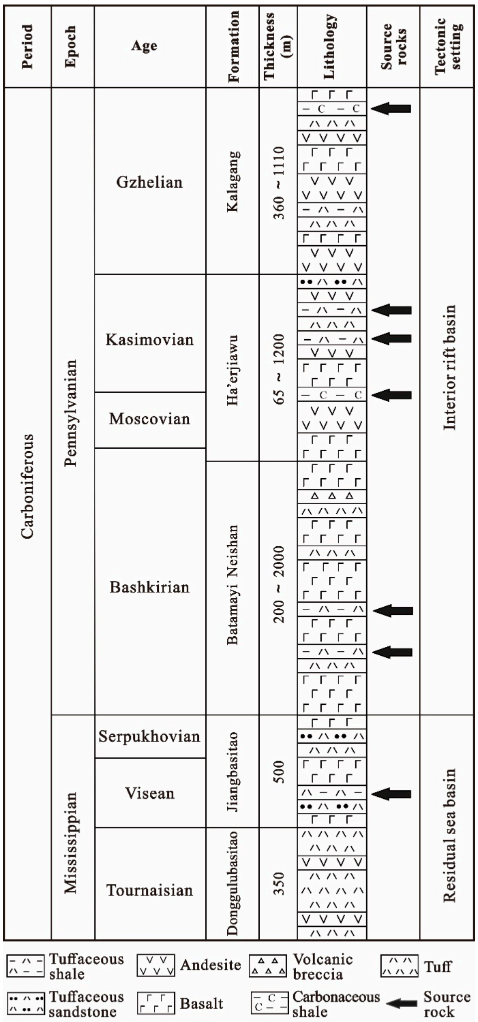

Figure 2. Generalized stratigraphic column of the Carboniferous strata in the Santanghu Basin with the source rock intervals labeled [24].

3. Samples and Analytical Methods

3.1. Samples

In this study, 10 core samples were collected from the Carboniferous Ha'erjiawu Formation black shales of well M38 for elemental geochemical analysis. Additionally, a total of 58 core samples from the Carboniferous Ha'erjiawu Formation black shales of 6 wells were utilized to determine the total organic carbon (TOC) contents, chloroform bitumen "A" contents, and Rock-Eval pyrolysis parameters. All the analyses were carried out by the test center of Petro-China Turpan-Hami Oilfield Company (Hami, China).

3.2. Analytical Methods

For elemental geochemical analysis, the black shale samples were ground into powder and subjected to a two-step digestion method (HNO_3-HNO_3: HF: $HClO_4$) to ensure retention of volatile elements in solution. Then, the element concentrations were determined using inductively coupled plasma optical emission spectrometry (ICP-OES, Thermo Scientific IRIS Intrepid II XSP, Waltham, MA, USA) according to the Chinese standard JY/T 015-1996. The geostandard materials GSR-5, GSR-6, and GSR-9 were used to monitor the analytical accuracy and precision. The analytical uncertainties range from 5 to 15% relative, contingent upon the concentrations of elements present in the samples.

The TOC contents were analyzed using a LECO CS-200 elemental analyzer after the finely powdered rock samples had been digested with diluted HCl (1:7 HCl:H_2O) at 70 °C for 2 h to remove inorganic carbon (carbonate), following Chinese national standard GB/T 19145-2003. Subsequently, the dried powder was weighed and burned in the elemental analyzer to determine TOC content. The analytical precision achieved was within ±0.1%.

Rock-Eval pyrolysis was conducted using a Rock-Eval OGE-II analyzer in accordance with the Chinese national standard (GB/T 18602-2012). The pulverized samples were heated at a programmed rate to obtain S_1, S_2, and Tmax. S_1 represents the free hydrocarbon content, while S_2 indicates the amount of hydrocarbons generated through thermal cracking. Tmax is defined as the temperature at which the maximum evolution of pyrolysis (S_2) peak occurs. Subsequently, the hydrogen index (HI = $S_2 \times 100/\text{TOC}$), production index (PI = $S_1/(S_1 + S_2)$), and petroleum generation potential (PG = $S_1 + S_2$) were calculated.

The chloroform bitumen "A" was determined using the widely accepted Soxhlet extraction method. The black shale samples were pulverized to a particle size of 100 mesh and subjected to a 72 h extraction with high purity chloroform, ensuring complete dissolution of chloroform bitumen "A" in the samples. The resulting extract was then weighed after undergoing reduced pressure distillation, concentration, and drying.

4. Results

4.1. Elemental Geochemistry

Table 1 presents the analytical results of elemental geochemistry for the black shales in the Ha'erjiawu Formation, while Figure 3 illustrates the concentration coefficients (i.e., ratio of element concentration in studied samples versus upper continental crust) for these samples.

Table 1. The elemental geochemistry results of the black shales from the Ha'erjiawu Formation in well M38.

Sample ID	**M38-1**	**M38-2**	**M38-3**	**M38-4**	**M38-5**	**M38-6**	**M38-7**	**M38-8**	**M38-9**	**M38-10**
Depth (m)	3038.13	3038.23	3038.43	3038.31	3039.46	3039.99	3040.05	3041.44	3041.59	3041.69
Na (%)	3.49	3.75	3.11	3.30	1.01	1.67	2.32	2.54	3.27	1.87
K (%)	0.06	0.16	0.67	0.46	1.30	2.31	2.43	0.11	0.13	1.69
Ti (%)	0.20	0.44	0.66	0.47	0.27	0.43	0.46	0.36	0.27	0.63
Fe (%)	3.30	7.31	10.58	6.81	3.10	5.01	4.51	13.21	5.09	8.53

Table 1. *Cont.*

Sample ID	M38-1	M38-2	M38-3	M38-4	M38-5	M38-6	M38-7	M38-8	M38-9	M38-10
Ca (%)	3.92	1.47	1.98	1.88	1.00	4.74	1.99	2.55	0.81	1.54
Mg (%)	0.36	1.16	1.99	1.18	0.12	0.51	0.41	0.37	0.22	0.25
Al (%)	9.35	12.28	10.56	12.22	4.80	13.41	10.60	7.10	6.97	7.04
Mn (ppm)	235.00	963.00	1856.00	1150.00	377.00	652.00	463.00	1676.00	456.00	1511.00
Li (ppm)	11.39	14.40	36.71	24.99	13.76	19.67	15.29	32.74	6.28	22.52
B (ppm)	1.70	1.54	3.14	1.99	2.44	2.02	1.83	3.77	3.39	2.40
Sc (ppm)	13.79	26.98	33.08	22.57	5.41	39.82	15.46	16.95	10.93	11.47
V (ppm)	162.00	186.00	312.00	166.00	97.49	124.00	155.00	466.00	216.00	201.00
Cr (ppm)	32.30	45.09	109.00	111.00	67.63	106.00	121.00	39.25	31.10	71.79
Ni (ppm)	29.33	52.71	45.41	56.10	19.61	30.74	53.13	30.04	42.00	17.63
Cu (ppm)	54.15	79.63	60.14	46.55	34.33	37.56	52.72	97.77	138.00	76.07
Zn (ppm)	60.84	71.24	102.00	86.80	46.62	84.35	76.28	85.38	75.98	73.43
Ga (ppm)	3.37	7.72	11.88	9.76	5.68	7.32	7.05	8.44	6.54	12.31
Sr (ppm)	197.00	175.00	209.00	264.00	850.00	1875.00	1681.00	128.00	101.00	156.00
Y (ppm)	29.33	16.08	23.54	9.93	1.51	21.67	4.26	24.08	14.03	0.88
Zr (ppm)	89.20	134.00	238.00	181.00	134.00	190.00	205.00	187.00	135.00	213.00
Ba (ppm)	65.70	254.00	380.00	218.00	559.00	1085.00	1006.00	73.25	54.78	101.00
Cd (ppm)	0.01	0.02	0.05	0.03	0.01	0.02	0.02	0.06	0.02	0.03
Mo (ppm)	6.97	8.46	6.08	7.53	3.80	9.54	6.38	5.09	4.89	3.96
Nb (ppm)	9.42	20.77	30.29	21.38	12.81	18.67	20.80	16.44	12.24	27.29
Rb (ppm)	6.62	5.88	7.03	8.87	28.57	63.05	56.55	4.32	3.41	5.26

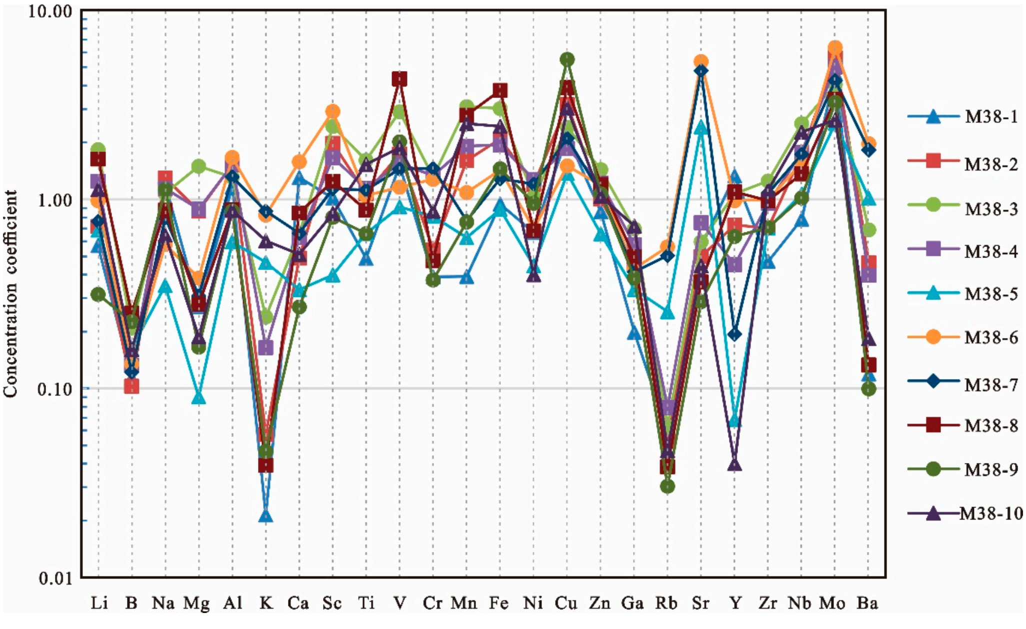

Figure 3. Concentration coefficients of trace elements, relative to the upper continental crust [28].

In comparison to the average values observed in the upper continental crust [28], all samples in this study exhibit notable enrichments in elements Cu and Mo, with concentration coefficients ranging from 1.37 to 5.52 (average 2.71), and from 2.53 to 6.36 (average 4.18), respectively. Conversely, there is clear evidence of depletion in elements B, K, Ga, and Rb across all samples, with concentration coefficients ranging from 0.10 to 0.25 (average 0.16), 0.02 to 0.87 (average 0.33), 0.20 to 0.72 (average 0.47), and 0.03 to 0.56 (average 0.17), respectively. Moreover, the majority of the samples demonstrate enrichments (concentration coefficient > 1) in elements such as Sc, V, Mn, Fe, and Nb, whereas depletions (concentration coefficient < 1) are observed in elements such as Mg, Ca, Cr, Ni, Sr, and Ba. However, the enrichment or depletion patterns of other measured elements are less discernible, as their concentration coefficients fluctuate around 1.

4.2. Bulk Organic Geochemical Parameters

The Ha'erjiawu Formation black shales were analyzed for the determination of TOC, chloroform bitumen "A", and Rock-Eval pyrolysis parameters (Table 2).

Table 2. The TOC, chloroform bitumen "A", and Rock-Eval pyrolysis parameters of the black shales from the Ha'erjiawu Formation.

Well ID	Sample ID	Depth (m)	TOC	S_1	S_2	Tmax	PG	PI	HI	OSI	Chloroform Bitumen "A" (wt%)
M38	M38-1	3040.00	3.48	1.22	6.14	449.00	7.36	0.17	176.44	35.06	
M38	M38-2	3041.00	10.90	3.85	53.79	439.00	57.64	0.07	493.49	35.32	
M38	M38-3	3042.00	1.97	1.17	2.25	446.00	3.42	0.34	114.21	59.39	
M38	M38-4	3042.40	3.61	1.03	12.93	442.00	13.96	0.07	358.17	28.53	
M38	M38-5	3039.48	14.43	10.22	54.72	443.00	64.94	0.16	379.21	70.82	
M38	M38-6	3039.58	4.84	1.39	10.06	445.00	11.45	0.12	207.85	28.72	
M38	M38-7	3039.97	4.08	1.55	7.48	448.00	9.03	0.17	183.33	37.99	0.41
M38	M38-8	3040.14	4.15	2.00	8.52	444.00	10.52	0.19	205.30	48.19	
M38	M38-9	3040.62	8.22	4.75	23.06	441.00	27.81	0.17	280.54	57.79	
M38	M38-10	3041.44	10.09	7.99	42.36	437.00	50.35	0.16	419.82	79.19	1.75
M38	M38-11	3041.63	13.45	7.99	62.55	441.00	70.54	0.11	465.06	59.41	
M38	M38-12	3041.93	14.86	8.14	66.62	441.00	74.76	0.11	448.32	54.78	
M38	M38-13	3042.19	5.78	1.46	9.29	446.00	10.75	0.14	160.73	25.26	
M38	M38-14	3042.50	4.91	3.40	18.49	443.00	21.89	0.16	376.58	69.25	0.60
M38	M38-15	3052.50	16.73	6.25	82.00	446.00	88.25	0.07	490.14	37.36	1.64
M38	M38-16	3085.00	21.84	12.54	76.68	447.00	89.22	0.14	351.10	57.42	0.95
M38	M38-17	3095.00	15.81	5.12	88.89	450.00	94.01	0.05	562.24	32.38	0.98
M38	M38-18	3132.00	17.53	8.26	95.06	449.00	103.32	0.08	542.27	47.12	1.25
M38	M38-19	3178.50	4.57	1.72	16.54	447.00	18.26	0.09	361.93	37.64	
M40	M40-1	2668.04	2.17	0.44	4.75	439.00	5.19	0.08	218.89	20.28	
M40	M40-2	2668.23	23.30	11.60	130.59	430.00	142.19	0.08	560.47	49.79	
M40	M40-3	2731.80	7.44	2.99	44.88	438.00	47.87	0.06	603.23	40.19	
M40	M40-4	2732.22	5.99	4.53	29.92	442.00	34.45	0.13	499.50	75.63	1.15
M40	M40-5	2732.86	5.57	7.01	27.45	440.00	34.46	0.20	492.82	125.85	1.95
M40	M40-6	2734.10	4.02	20.12	22.39	431.00	42.51	0.47	556.97	500.50	
M42	M42-1	3986.46	5.41	0.86	2.11	496.00	2.97	0.29	39.00	15.90	
M42	M42-2	3987.50	7.67	2.41	6.85	474.00	9.26	0.26	89.31	31.42	0.26
M42	M42-3	3988.50	7.13	1.04	6.77	473.00	7.81	0.13	94.95	14.59	
M42	M42-4	3988.90	1.67	1.08	1.95	471.00	3.03	0.36	116.77	64.67	
M42	M42-5	3989.50	0.45	0.08	1.70	446.00	1.78	0.04	377.78	17.78	
M361	M361-1	3155.40	0.36	0.09	0.59	443.00	0.68	0.13	163.89	25.00	
M361	M361-2	3156.20	1.08	0.29	2.92	446.00	3.21	0.09	270.37	26.85	0.23
M361	M361-3	3157.10	0.82	0.30	1.47	446.00	1.77	0.17	179.27	36.59	
M361	M361-4	3157.40	19.06	15.79	94.19	445.00	109.98	0.14	494.18	82.84	
M361	M361-5	3158.00	17.75	18.37	115.20	447.00	133.57	0.14	649.01	103.49	
M361	M361-6	3159.10	1.40	0.99	5.18	443.00	6.17	0.16	370.00	70.71	
M361	M361-7	3159.72	3.72	4.13	15.89	439.00	20.02	0.21	427.15	111.02	0.32
M361	M361-8	3162.50	0.10	0.05	0.11	444.00	0.16	0.31	110.00	50.00	
ND201	ND201-1	3271.00	2.24	1.02	4.53	446.00	5.55	0.18	202.23	45.54	
ND201	ND201-2	3275.00	14.30	2.45	83.84	448.00	86.29	0.03	586.29	17.13	1.22
ND201	ND201-3	3278.00	12.41	3.12	75.57	447.00	78.69	0.04	608.94	25.14	
ND201	ND201-4	3283.00	6.58	2.06	27.77	447.00	29.83	0.07	422.04	31.31	
ND201	ND201-5	3290.00	4.95	1.73	21.51	445.00	23.24	0.07	434.55	34.95	
ND201	ND201-6	3300.00	8.84	2.22	52.87	448.00	55.09	0.04	598.08	25.11	
ND201	ND201-7	3304.00	7.88	1.43	47.57	447.00	49.00	0.03	603.68	18.15	
ND201	ND201-8	3307.00	6.96	2.16	34.48	445.00	36.64	0.06	495.40	31.03	0.72

Table 2. *Cont.*

Well ID	Sample ID	Depth (m)	TOC	S_1	S_2	Tmax	PG	PI	HI	OSI	Chloroform Bitumen "A" (wt%)
ND201	ND201-9	3317.00	3.75	1.26	14.08	448.00	15.34	0.08	375.47	33.60	
ND201	ND201-10	3321.00	3.20	0.74	12.19	449.00	12.93	0.06	380.94	23.13	
ND201	ND201-11	3324.00	4.58	1.43	20.69	449.00	22.12	0.06	451.75	31.22	
ND201	ND201-12	3328.00	3.42	1.11	15.32	451.00	16.43	0.07	447.95	32.46	
ND201	ND201-13	3336.00	4.02	1.10	18.10	449.00	19.20	0.06	450.25	27.36	
ND201	ND201-14	3339.00	4.08	1.53	18.20	451.00	19.73	0.08	446.08	37.50	0.43
TC3	TC3-1	3084.00	1.50	0.18	2.52	441.00	2.70	0.07	168.00	12.00	
TC3	TC3-2	3084.50	1.97	0.22	4.02	438.00	4.24	0.05	204.06	11.17	0.13
TC3	TC3-3	3085.00	2.07	0.33	5.08	438.00	5.41	0.06	245.41	15.94	
TC3	TC3-4	3085.50	16.25	1.79	116.38	431.00	118.17	0.02	716.18	11.02	
TC3	TC3-5	3086.00	1.52	0.20	2.34	440.00	2.54	0.08	153.95	13.16	
TC3	TC3-6	3088.00	1.61	0.33	3.45	438.00	3.78	0.09	214.29	20.50	

TOC = Total organic carbon (wt%); S_1 = Rock-Eval measured free hydrocarbons (mg HC/g rock); S_2 = amount of hydrocarbons that formed during thermal pyrolysis (mg HC/g rock); Tmax = temperature maximum (°C); PG: petroleum generation potential = $S_1 + S_2$, (mg HC/g rock); PI: production index = $S_1/(S_1 + S_2)$; HI: hydrogen index = $(S_2/\mathrm{TOC}) \times 100$, (mg HC/g TOC); OSI: oil saturation index = $(S_1/\mathrm{TOC}) \times 100$, (mg HC/g TOC).

The TOC content of the samples exhibits a wide range, spanning from 0.1 to 23.3 wt%, with an average value of 7.04 wt% (n = 58). Notably, a significant majority of the samples, accounting for approximately 81.03%, possess TOC values equal to or exceeding 2%, indicating a remarkable abundance of organic matter. The chloroform bitumen "A" values of the samples exhibit a wide range, spanning from 0.13 to 1.95 wt%, with an average concentration of 0.87 wt% (n = 16). Notably, among the 16 data points for chloroform bitumen "A", a significant majority of 11 measurements surpass or equal the threshold of $\geq$0.60 wt%, accounting for approximately 68.75%. Rock-Eval pyrolysis analysis reveals that the S_1 value of the samples exhibits a wide range from 0.05 to 20.12 mg HC/g rock, with an average value of 3.60 mg HC/g rock (n = 58). The S_2 and PG values for the samples exhibit a wide range, spanning from 0.11 to 130.59 mg HC/g rock, and 0.16 to 142.19 mg HC/g rock, respectively, with average values of 31.60 mg HC/g rock and 35.20 mg HC/g rock (n = 58), respectively. The HI values of the samples range from 39.00 to 716.18 mg HC/g TOC, with an average value of 363.72 mg HC/g TOC (n = 58). The Tmax value serves as an indicator of thermal maturity, ranging from 430 to 496 °C, with an average of 446 °C (n = 58). Except for samples from well M42 that have experienced significant burial depth, all other samples exhibit Tmax values below 460 °C. The OSI values of the samples exhibit a wide range, spanning from 11.02 to 500.50 mg HC/g TOC, with an average value of 49.35 mg HC/g TOC (n = 58). This indicates that the oil content in the samples varies significantly.

5. Discussion

5.1. Paleoenvironmental Conditions

The paleoenvironmental conditions of shale can be discerned through its elemental geochemical composition [29–33]. In general, the B content and certain geochemical indicators, such as Sr/Ba, Rb/K, and B/Ga ratios, may serve as proxies for paleosalinity [22,34–36]. The Sr/Ba ratio serves as a widely employed proxy for paleosalinity in carbonate-free shale [36,37]. Previous research has indicated that the Ha'erjiawu Formation black shales contain a certain amount of carbonate minerals [26], rendering the use of Sr/Ba ratio unsuitable for paleosalinity evaluation. Although there remains an ongoing debate regarding the origin of boron in sedimentary rocks, it has been observed that there is a positive correlation between boron concentration and water salinity [34,36,38,39]. The concentration of the element B in the black shale samples from the Ha'erjiawu Formation ranges from 1.54 to 3.77 ppm, which is significantly lower compared to that found in saline and brackish water environments. The Rb/K and B/Ga ratios have been widely established as excellent paleosalinity proxies [22,29,40]. In general, Rb/K ratios greater than 0.006, between 0.004 and 0.006, and less than or equal to 0.0028 correspond to saline, brackish, and freshwater environments, respectively [41]. The B/Ga ratios exceeding 4 are indicative of brackish-saline environments, while those ranging from 2.5 to 4.0 suggest mildly brackish conditions, and values below 2.5 imply freshwater settings [42]. In this study, the Rb/K and B/Ga ratios range from 0.0003 to 0.0110, with an average of 0.0032, and from 0.19 to 0.52, with an average of 0.33, respectively. These consistent findings strongly suggest that the black shales of the Ha'erjiawu Formation were deposited in freshwater environments (Figure 4a). In the B–Ga–Rb diagram (Figure 4b), all the samples are situated within the realm of a freshwater environment, thereby signifying that the deposition of the Ha'erjiawu Formation black shales occurred in water columns characterized by low salinity.

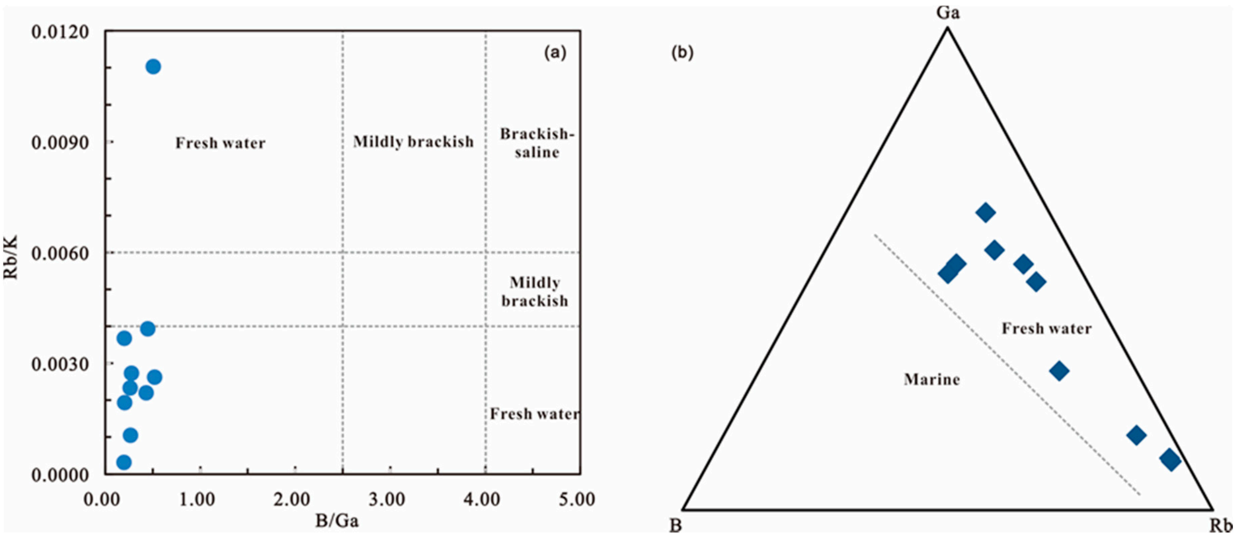

Figure 4. Element discrimination plots illustrating paleosalinity for the Ha'erjiawu Formation black shale samples. (**a**) Rb/K vs. B/Ga; (**b**) B–Ga–Rb diagram [43].

Diverse climatic conditions exert distinct influences on the decomposition, migration, and enrichment behaviors of geochemical elements with varying characteristics [44–47]. Hence, the paleoclimatic conditions can be deduced from the elemental composition of sedimentary rocks [48–50]. For example, the utilization of Ga/Rb, Sr/Cu, and K_2O/Al_2O_3 ratios as geochemical proxies in shales has long been employed to reconstruct the climatic conditions in geologic history [46,50–52]. Generally, a high Ga/Rb ratio (>0.25) and low K_2O/Al_2O_3 ratio (<0.2) suggest intense chemical weathering associated with warm and humid climatic conditions, whereas a low Ga/Rb ratio (<0.25) and high K_2O/Al_2O_3 ratio (>0.2) indicate weak weathering linked to dry and cold climatic conditions [46]. The Sr/Cu ratio ranging from 1.3 to 5.0 is indicative of a humid and warm climate, whereas a Sr/Cu ratio exceeding 5.0 suggests an arid climate [52]. In this study, the geochemical proxies reveal that the majority of samples from the Ha'erjiawu Formation black shales were deposited under warm and humid climatic conditions, while a minority of samples were formed in dry and cold climatic conditions (Figure 5). This climate fluctuation may be attributed to the influence of synsedimentary volcanic activity or the Late Paleozoic glaciation [53,54]. In fact, previous studies have demonstrated that the Santanghu region and its surrounding areas underwent a shift from a wet to dry climate during the Carboniferous period, with the Ha'erjiawu Formation situated in the transitional phase [55,56], which aligns with the findings of this study. Further investigation is required to explore the specific circumstances of this climatic event, particularly its genetic association with the Late Paleozoic glaciation.

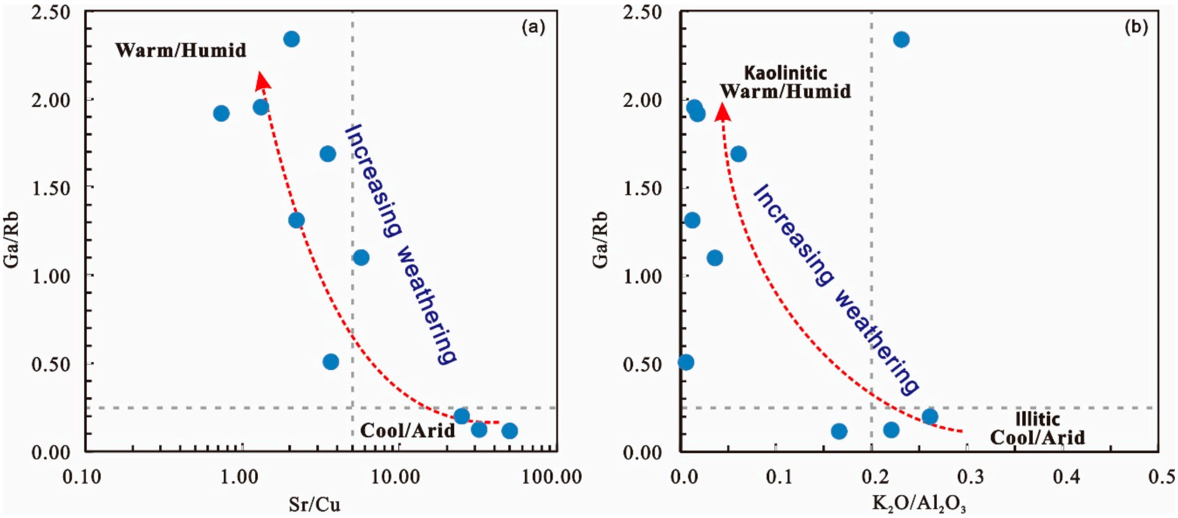

Figure 5. Crossplots of paleoclimatic proxies for the Ha'erjiawu Formation black shale samples. (**a**) Ga/Rb vs. Sr/Cu; (**b**) Ga/Rb vs. K_2O/Al_2O_3.

Redox conditions are crucial for understanding paleoenvironmental conditions, and have a significant impact on the geochemical properties and behaviors of redox-sensitive elements [57–60]. Hence, certain geochemical indices pertaining to redox-sensitive elements, such as the V/Cr, V/(V + Ni), V/Al, and Mo/Al ratios, serve as valuable indicators for reconstructing the redox conditions of ancient sedimentary sequences [57–59,61–63]. Elements V and Mo have a predilection for enrichment in reducing environments, as opposed to Cr and Ni. Consequently, the ratios of V/Cr, V/(V + Ni), V/Al, and Mo/Al increase with decreasing water oxidation degree [57–59,64]. Previous studies have proposed thresholds for quantitatively classifying redox conditions based on these indicators, although there is no consensus on the applicability of these thresholds in nonmarine environments [22,58,63,65]. In this study, the redox indicators of the samples fall within a range between oxic and anoxic conditions (Figure 6), signifying that the Ha'erjiawu Formation was predominantly deposited in dysoxic environments, which is consistent with reducing depositional settings inferred from thinly laminated black shales and widespread occurrence of framboidal pyrite [26].

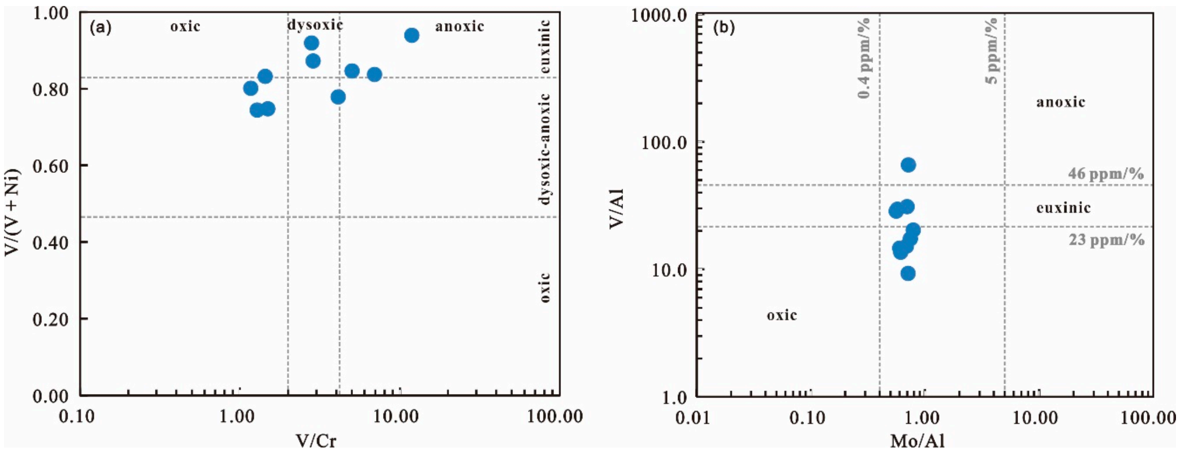

Figure 6. Crossplots of paleoredox proxies for the Ha'erjiawu Formation black shale samples. (**a**) V/(V + Ni) vs. V/Cr; (**b**) V/Al vs. Mo/Al.

In general, our data indicate that the black shales of the Carboniferous Ha'erjiawu Formation in the Santanghu Basin were formed in a lacustrine environment characterized by low salinity and a relatively mild redox state. The prevailing climate during the deposition of the Ha'erjiawu Formation in the Carboniferous period was marked by alternating warm-wet and cold-dry phases. These findings gain further support from recent studies that have employed both inorganic geochemistry and biomarkers [26]. Nevertheless, the previous assertion that the Ha'erjiawu Formation was formed in a marine environment solely based on biomarkers raises doubts and warrants further examination [24].

5.2. Shale Oil Potential

In recent years, remarkable advancements have been achieved in the exploration of shale oil within the Santanghu Basin [22,25,66–68]. However, previous shale oil exploration in the Santanghu Basin primarily focused on the Permian Lucaogou Formation, with comparatively less emphasis placed on the Carboniferous Ha'erjiawu Formation [25,26]. Considering that the Ha'erjiawu Formation serves as the primary source rock for the commercially productive oil reservoirs above it [24,26], a more comprehensive evaluation of the shale oil potential in the Ha'erjiawu Formation is warranted.

Source rocks serve as the paramount prerequisite for the accumulation and enrichment of shale oil [2,7]. The abundance of organic matter constitutes the primary influencing factors on the hydrocarbon generation capacity in shale. The TOC content (0.1–23.3 wt%, avg. 7.04 wt%, $n = 58$) of the samples demonstrates that Ha'erjiawu Formation black shales possess remarkably high levels of organic matter abundance. The concurrence of high S_2 and PG values with high TOC content suggests that the Ha'erjiawu Formation black shales are good potential hydrocarbon-generative source rocks. In the plots of TOC content vs. PG, and chloroform bitumen "A" vs. TOC content (Figure 7), most of the samples fall into the categories of good to excellent source rocks.

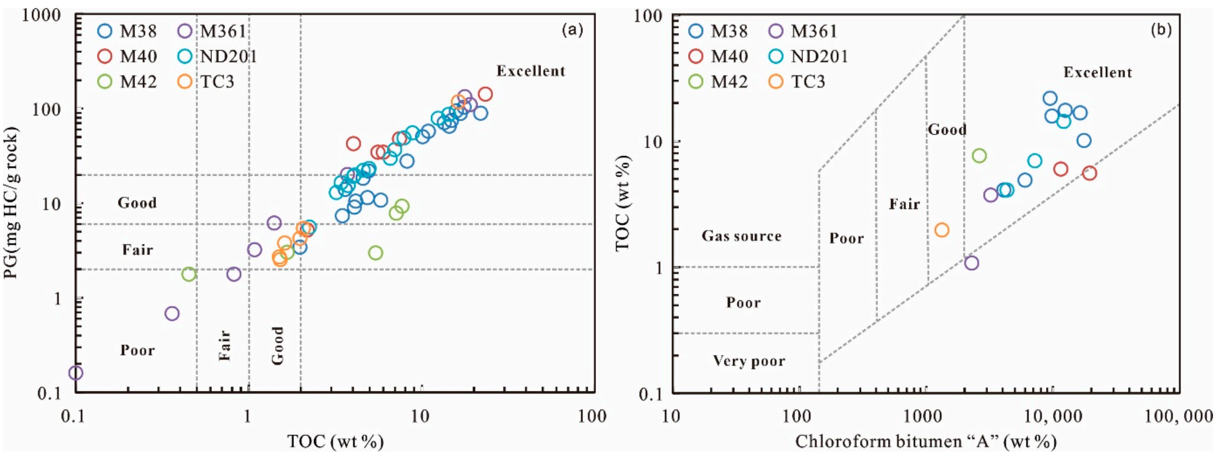

Figure 7. Crossplots of PG vs. TOC (**a**) and TOC vs. chloroform bitumen "A" (**b**) showing the source rock potential for the analyzed Ha'erjiawu Formation black shale samples.

Apart from the abundance of organic matter present, the type of organic matter is another crucial factor required for predicting the capacity of hydrocarbon generation [22,69]. We employ crossplots of HI vs. Tmax and S_2 vs. TOC to differentiate between various organic matter types present in the black shales of the Ha'erjiawu Formation. The cross-plots suggest that the kerogen of the Ha'erjiawu Formation black shales is predominantly composed of type II, as depicted in Figure 8. This indicates that the organic matter is a mixture of aquatic and terrestrial organisms, consistent with previously reported biomarker compounds [24]. Consequently, most samples from the Ha'erjiawu Formation are classified as type II, and have great potential to generate substantial amounts of oil under appropriate conditions of burial and heating.

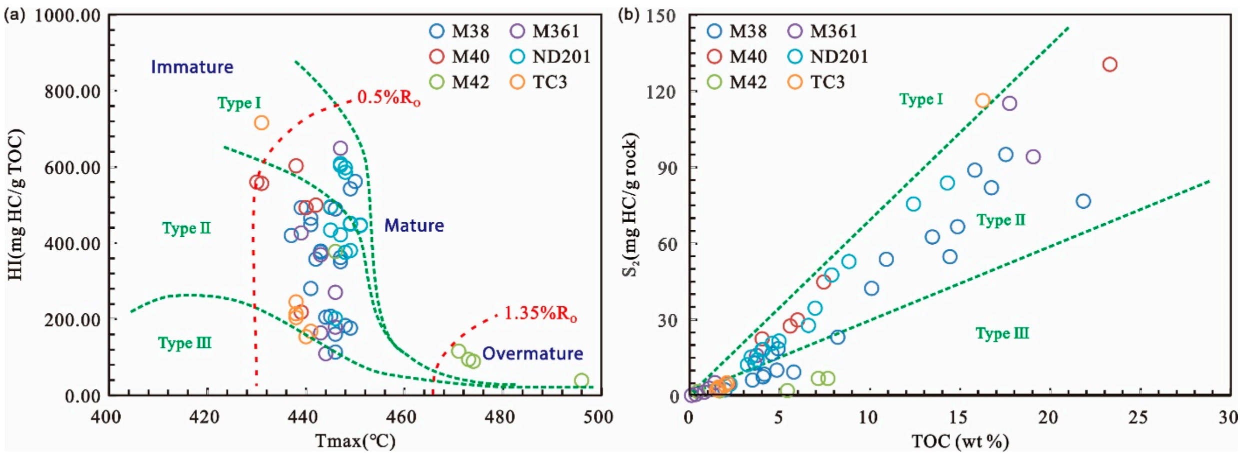

Figure 8. Crossplots of HI vs. Tmax (**a**) and S_2 vs. TOC (**b**) showing the kerogen type for the analyzed Ha'erjiawu Formation black shale samples.

The thermal maturity of organic matter in shale is a crucial factor that influences both the quality and quantity of hydrocarbon products, rendering it an indispensable parameter for assessing the potential of shale oil [70,71]. It is widely acknowledged that the Rock-Eval Tmax value exhibits a linear correlation with the maturation level of organic matter, thus rendering the Tmax value as a commonly employed tool for expeditious assessment of thermal maturity in source rocks [72,73]. In this study, the majority of samples exhibit Tmax values ranging from 430 to 460 °C (with an average of 443 °C), with the exception of a few samples extracted from well M42 that display anomalously high Tmax values spanning between 471 and 496 °C (averaging at 478 °C). The observed Tmax values indicate that most of the Ha'erjiawu Formation has reached early to mature stages, while only a small portion being over-mature, due to either deep burial or subsequent magmatism. The production index (PI) can also serve as an indicator of the thermal maturity of organic matter to a certain extent. The crossplot of Tmax vs. PI reveals that the majority of samples fall within the early mature to mature stage (Figure 9). These maturity indexes based on Rock-Eval pyrolysis are in accordance with the previously reported vitrinite reflectance values (most falling within the range of 0.76–0.90, except for one sample from well M42 which measures 1.74 [26]), indicating that the Ha'erjiawu Formation is predominantly at its peak stage of oil generation.

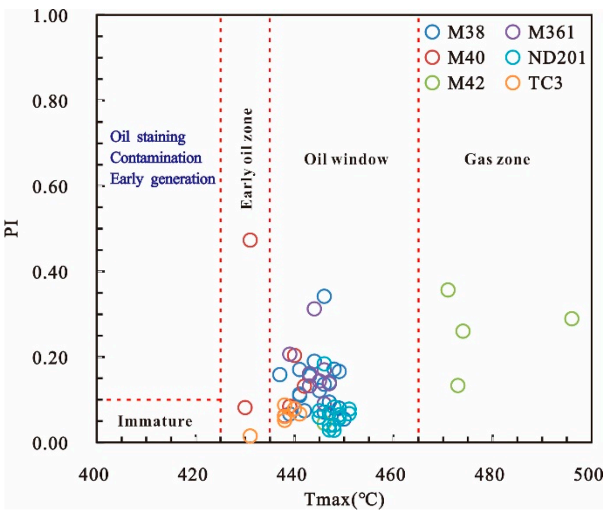

Figure 9. Tmax vs. PI plot showing the thermal maturity of organic matter for the analyzed Ha'erjiawu Formation black shale samples.

The oil content stands as a pivotal parameter in evaluating the potential of shale oil, for it determines the feasibility of commercial production [2,7,74,75]. Drawing on extensive experience in shale oil exploration across the United States, Jarvie [2] proposed an index known as the oil saturation index (OSI = S_1/TOC × 100) to assess the producible oil content of shale. It is widely believed that when the OSI value is >100 mg HC/g TOC, the shale contains producible free oil; when the OSI value is in the range of 75 to 100 mg HC/g TOC, the shale oil has abundant adsorbed hydrocarbons. In this study, the OSI values of the samples ranged from 11.02 to 500.50 mg HC/g TOC, with four samples exceeding 100 mg HC/g TOC. This suggests that certain intervals within the Ha'erjiawu Formation may contain substantial amounts of producible movable oil (Figure 10a). It is important to note that the OSI is a relative measure, and therefore has limitations in assessing shale oil content [7,22]. As S_1 can be considered as a more absolute indicator of oil content in shale [19], Lu et al. [76] proposed a grading evaluation criterion based on TOC and S_1 for determining shale oil potential. Based on this grading evaluation criterion, the majority of our samples are classified into Zone II (TOC > 0.5 wt%; S_1 > 2 mg HC/g rock) and Zone III (TOC > 2 wt%; S_1 < 2 mg HC/g rock), with a minority falling into Zone I (TOC < 2 wt%; S_1 < 2 mg HC/g rock). This suggests that the majority of the Ha'erjiawu Formation black shales are classified as enriched and potential shale oil resources, while a minority of black shales are categorized as ineffective shale oil resources (Figure 10b).

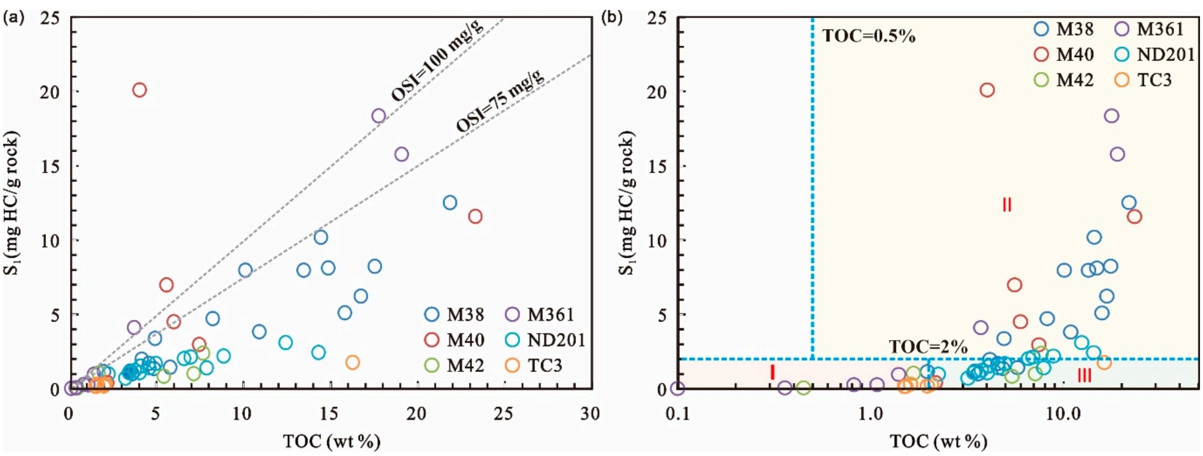

Figure 10. (**a**) OSI values of the Ha'erjiawu Formation black shale samples. (**b**) Oil and TOC content classification of the shale oil into ineffective (I), enriched (II), and potential resources (III).

Shale, known for its inherently low permeability, necessitates the implementation of hydraulic fracturing techniques to enhance its permeability and facilitate the extraction of shale oil [77]. The development of extensive fracture networks is intimately linked to the brittleness of shale, thus making brittleness a crucial factor in evaluating the potential for shale oil [78,79]. There exist two approaches to appraise rock brittleness, namely, mineral composition analyses and mechanical elastic parameters, with the former being predominantly employed in the early stage of shale oil exploration [80,81]. Brittle mineral content is frequently employed to evaluate brittleness, albeit the standards for identifying brittle minerals may differ slightly [80]. A recent study has revealed that despite significant variations in mineral composition, the Ha'erjiawu Formation black shales exhibit an average brittle mineral content (including quartz, feldspar, and carbonate minerals) exceeding 60% [26]. The high brittle mineral content of the Ha'erjiawu Formation black shales suggests that it is likely to exhibit a favorable response to hydraulic fracturing.

In summary, the abundance, type, and thermal maturity of organic matter in the Ha'erjiawu Formation black shales suggest that it has the potential to yield copious amounts of oil for shale oil enrichment. Moreover, the abundant presence of brittle minerals in the Ha'erjiawu Formation black shales renders it conducive to hydraulic fracturing for shale oil exploitation. Although the Ha'erjiawu Formation displays promising potential for shale oil, only a limited number of samples in this study exhibit high OSI values. Therefore, the key to successful exploration and development of shale oil in the Carboniferous Ha'erjiawu Formation in Santanghu Basin lies in identifying intervals with high oil content.

6. Conclusions

Through combined elemental and organic geochemical analyses, the paleoenvironmental conditions and shale oil potential of the Carboniferous Ha'erjiawu Formation black shales in the Santanghu Basin were investigated. Our findings unveil that these black shales were deposited in water columns with low salinity and dysoxic conditions, as indicated by paleosalinity and redox proxies. The climatic indicators suggest that the Santanghu Basin was characterized by an oscillating climate of warm-humid/cold-dry during the deposition of black shales in the Ha'erjiawu Formation. This fluctuation in climate may be attributed to either synsedimentary volcanic activity or the Late Paleozoic glaciation.

The organic geochemical analyses reveal that the Ha'erjiawu Formation black shales, characterized by an abundance of type II kerogen in the early mature to mature stage, possess a substantial capacity for oil generation. Although the Ha'erjiawu Formation black shales have the potential to provide abundant oil for shale oil enrichment, the analyzed samples exhibit significant variability in their oil content, with only a select few containing mobile oil. The identification of high oil-bearing intervals will be crucial for the exploration and development of shale oil in the future, given the Ha'erjiawu Formation black shales' abundant brittle minerals content.

Author Contributions: Conceptualization, S.Z.; data curation, H.L.; funding acquisition, S.Z.; investigation, Z.F., H.L., J.G., H.S., L.Z. and Y.G.; methodology, C.L.; project administration, S.Z., C.L. and H.L.; visualization, Z.F.; writing—original draft, S.Z. and W.D.; writing—review and editing, S.Z. and W.D. All authors have read and agreed to the published version of the manuscript.

Funding: This work is financially supported by the National Natural Science Foundation of China (42102128 and 42202175), the National Science and Technology Major Project of China (2011ZX05044), and Sinopec science and technology project (P14150).

Data Availability Statement: The data presented in this study are available in the main text.

Acknowledgments: We thank PetroChina Turpan-Hami Oilfield Company for kindly providing subsurface datasets, and for the permission to publish the results of this study.

Conflicts of Interest: The authors declare no conflict of interest.

References

1. Katz, B.; Lin, F. Lacustrine Basin Unconventional Resource Plays: Key Differences. *Mar. Pet. Geol.* **2014**, *56*, 255–265. [CrossRef]
2. Jarvie, D.M. Shale Resource Systems for Oil and Gas: Part 2—Shale-Oil Resource Systems. In *Shale Reservoir—Giant Resources for the 21st Century: AAPG Memoir 97*; AAPG: Tulsa, OK, USA, 2012; pp. 89–119. [CrossRef]
3. Zou, C.; Zhu, R.; Chen, Z.-Q.; Ogg, J.G.; Wu, S.; Dong, D.; Qiu, Z.; Wang, Y.; Wang, L.; Lin, S.; et al. Organic-Matter-Rich Shales of China. *Earth-Sci. Rev.* **2019**, *189*, 51–78. [CrossRef]
4. Wang, M.; Li, M.; Li, J.-B.; Xu, L.; Zhang, J.-X. The Key Parameter of Shale Oil Resource Evaluation: Oil Content. *Pet. Sci.* **2022**, *19*, 1443–1459. [CrossRef]
5. Al-Shami, T.M.; Jufar, S.R.; Kumar, S.; Abdulelah, H.; Abdullahi, M.B.; Al-Hajri, S.; Negash, B.M. A Comprehensive Review of Interwell Interference in Shale Reservoirs. *Earth-Sci. Rev.* **2023**, *237*, 104327. [CrossRef]
6. Jin, Z.; Zhu, R.; Liang, X.; Shen, Y. Several Issues Worthy of Attention in Current Lacustrine Shale Oil Exploration and Development. *Pet. Explor. Dev.* **2021**, *48*, 1471–1484. [CrossRef]
7. Hu, T.; Pang, X.; Jiang, F.; Wang, Q.; Liu, X.; Wang, Z.; Jiang, S.; Wu, G.; Li, C.; Xu, T.; et al. Movable Oil Content Evaluation of Lacustrine Organic-Rich Shales: Methods and a Novel Quantitative Evaluation Model. *Earth-Sci. Rev.* **2021**, *214*, 103545. [CrossRef]
8. Wang, X.; Zhang, G.; Tang, W.; Wang, D.; Wang, K.; Liu, J.; Du, D. A Review of Commercial Development of Continental Shale Oil in China. *Energy Geosci.* **2022**, *3*, 282–289. [CrossRef]
9. Liu, B.; Wang, H.; Fu, X.; Bai, Y.; Bai, L.; Jia, M.; He, B. Lithofacies and Depositional Setting of a Highly Prospective Lacustrine Shale Oil Succession from the Upper Cretaceous Qingshankou Formation in the Gulong Sag, Northern Songliao Basin, Northeast China. *Am. Assoc. Pet. Geol. Bull.* **2019**, *103*, 405–432. [CrossRef]

10. Zhang, P.; Misch, D.; Hu, F.; Kostoglou, N.; Sachsenhofer, R.F.; Liu, Z.; Meng, Q.; Bechtel, A. Porosity Evolution in Organic Matter-Rich Shales (Qingshankou Fm.; Songliao Basin, NE China): Implications for Shale Oil Retention. *Mar. Pet. Geol.* **2021**, *130*, 105139. [CrossRef]
11. Li, M.; Chen, Z.; Ma, X.; Cao, T.; Qian, M.; Jiang, Q.; Tao, G.; Li, Z.; Song, G. Shale Oil Resource Potential and Oil Mobility Characteristics of the Eocene-Oligocene Shahejie Formation, Jiyang Super-Depression, Bohai Bay Basin of China. *Int. J. Coal Geol.* **2019**, *204*, 130–143. [CrossRef]
12. Song, Y.; Ye, X.; Shi, Q.; Huang, C.; Cao, Q.; Zhu, K.; Cai, M.; Ren, S.; Sun, L. A Comparative Study of Organic-Rich Shale from Turbidite and Lake Facies in the Paleogene Qikou Sag (Bohai Bay Basin, East China): Organic Matter Accumulation, Hydrocarbon Potential and Reservoir Characterization. *Palaeogeogr. Palaeoclimatol. Palaeoecol.* **2022**, *594*, 110939. [CrossRef]
13. Hou, Y.; Wang, F.; He, S.; Dong, T.; Wu, S. Properties and Shale Oil Potential of Saline Lacustrine Shales in the Qianjiang Depression, Jianghan Basin, China. *Mar. Pet. Geol.* **2017**, *86*, 1173–1190. [CrossRef]
14. Li, M.; Chen, Z.; Cao, T.; Ma, X.; Liu, X.; Li, Z.; Jiang, Q.; Wu, S. Expelled Oils and Their Impacts on Rock-Eval Data Interpretation, Eocene Qianjiang Formation in Jianghan Basin, China. *Int. J. Coal Geol.* **2018**, *191*, 37–48. [CrossRef]
15. Zou, C.; Pan, S.; Horsfield, B.; Yang, Z.; Hao, S.; Liu, E.; Zhang, L. Oil Retention and Intrasource Migration in the Organic-Rich Lacustrine Chang 7 Shale of the Upper Triassic Yanchang Formation, Ordos Basin, Central China. *Am. Assoc. Pet. Geol. Bull.* **2019**, *103*, 2627–2663. [CrossRef]
16. Chen, Y.; Zhu, Z.; Zhang, L. Control Actions of Sedimentary Environments and Sedimentation Rates on Lacustrine Oil Shale Distribution, an Example of the Oil Shale in the Upper Triassic Yanchang Formation, Southeastern Ordos Basin (NW China). *Mar. Pet. Geol.* **2019**, *102*, 508–520. [CrossRef]
17. Wei, G.; Wang, W.; Feng, L.; Tan, X.; Yu, C.; Zhang, H.; Zhang, Z.; Wang, S. Geological Characteristics and Exploration Prospect of Black Shale in the Dongyuemiao Member of Lower Jurassic, the Eastern Sichuan Basin, China. *Front. Earth Sci.* **2021**, *9*, 765568. [CrossRef]
18. Yuan, X.; Zhang, K.; Peng, J.; Li, B.; Han, F.; Chen, X.; Zheng, Z.; Ruan, J.; Ye, L.; Wang, Z.; et al. Study on Characteristics of Oil and Gas Occurrence and Reservoir Space of Medium-High Maturity Continental Shale—A Case Study of Middle Jurassic Lianggaoshan Formation in Fuling Block, Southeast of Sichuan Basin, South China. *Front. Earth Sci.* **2022**, *10*, 1032018. [CrossRef]
19. Li, W.; Cao, J.; Zhi, D.; Tang, Y.; He, W.; Wang, T.; Xia, L. Controls on Shale Oil Accumulation in Alkaline Lacustrine Settings: Late Paleozoic Fengcheng Formation, Northwestern Junggar Basin. *Mar. Pet. Geol.* **2021**, *129*, 105107. [CrossRef]
20. Qiu, Z.; Tao, H.; Zou, C.; Wang, H.; Ji, H.; Zhou, S. Lithofacies and Organic Geochemistry of the Middle Permian Lucaogou Formation in the Jimusar Sag of the Junggar Basin, NW China. *J. Pet. Sci. Eng.* **2016**, *140*, 97–107. [CrossRef]
21. Zhang, S.; Liu, C.; Liang, H.; Jia, L.; Bai, J.; Zhang, L.; Wang, J. Mineralogical Composition and Organic Matter Characteristics of Lacustrine Fine-Grained Volcanic-Hydrothermal Sedimentary Rocks: A Data-Driven Analytics for the Second Member of Permian Lucaogou Formation, Santanghu Basin, NW China. *Mar. Pet. Geol.* **2021**, *126*, 104920. [CrossRef]
22. Zhang, S.; Liu, C.; Liang, H.; Wang, J.; Bai, J.; Yang, M.; Liu, G.; Huang, H.; Guan, Y. Paleoenvironmental Conditions, Organic Matter Accumulation, and Unconventional Hydrocarbon Potential for the Permian Lucaogou Formation Organic-Rich Rocks in Santanghu Basin, NW China. *Int. J. Coal Geol.* **2018**, *185*, 44–60. [CrossRef]
23. Liu, B.; Lv, Y.; Zhao, R.; Tu, X.; Guo, X.; Shen, Y. Formation Overpressure and Shale Oil Enrichment in the Shale System of Lucaogou Formation, Malang Sag, Santanghu Basin, NW China. *Pet. Explor. Dev.* **2012**, *39*, 744–750. [CrossRef]
24. Song, D.; He, D.; Wang, S. Source Rock Potential and Organic Geochemistry of Carboniferous Source Rocks in Santanghu Basin, NW China. *J. Earth Sci.* **2013**, *24*, 355–370. [CrossRef]
25. Liang, S.; Luo, Q.; Wang, R.; Chen, X.; Yang, B.; Ma, Q.; Liang, H. Geological Characteristics and Exploration Practice of Unconventional Permian Oil Resources in the Santanghu Basin. *China Pet. Explor.* **2019**, *24*, 624–635. [CrossRef]
26. Li, T.-J.; Huang, Z.-L.; Chen, X.; Li, X.-N.; Liu, J.-T. Paleoenvironment and Organic Matter Enrichment of the Carboniferous Volcanic-Related Source Rocks in the Malang Sag, Santanghu Basin, NW China. *Pet. Sci.* **2021**, *18*, 29–53. [CrossRef]
27. Liang, H.; Li, X.; Ma, Q.; Liang, H.; Luo, Q.; Chen, X.; Bai, G.; Zhang, Q.; Meng, Y. Geological Features and Exploration Potential of Permian Tiaohu Formation Tight Oil, Santanghu Basin, NW China. *Pet. Explor. Dev.* **2014**, *41*, 616–627. [CrossRef]
28. McLennan, S.M. Relationships between the Trace Element Composition of Sedimentary Rocks and Upper Continental Crust. *Geochem. Geophys. Geosyst.* **2001**, *2*, 1021. [CrossRef]
29. Bai, J.; Zhang, S.; Liu, C.; Jia, L.; Luo, K.; Jiang, T.; Peng, H. Mineralogy and Geochemistry of the Middle Permian Pingdiquan Formation Black Shales on the Eastern Margin of the Junggar Basin, North-west China: Implications for Palaeoenvironmental and Organic Matter Accumulation Analyses. *Geol. J.* **2022**, *57*, 1989–2006. [CrossRef]
30. Bai, J.; Liu, C.; Zhang, S.; LU, J.; Sun, J. Zircon U-Pb Geochronology and Geochemistry of Basalts from the Qi'eshan Group in the Southern Turpan-Hami Basin, East Tianshan: Constraints on Closure Time of the North Tianshan Ocean. *Acta Petrol. Sin.* **2018**, *34*, 2995–3010.
31. Schultz, R.B.; Rimmer, S.M. Geochemistry of Organic-Rich Shales: New Perspectives. *Chem. Geol.* **2004**, *206*, 163–165. [CrossRef]
32. Hatch, J.R.; Leventhal, J.S. Relationship between Inferred Redox Potential of the Depositional Environment and Geochemistry of the Upper Pennsylvanian (Missourian) Stark Shale Member of the Dennis Limestone, Wabaunsee County, Kansas, U.S.A. *Chem. Geol.* **1992**, *99*, 65–82. [CrossRef]

33. Zhang, K.; Liu, R.; Bai, E.; Zhao, Z.; Peyrotty, G.; Fathy, D.; Chang, Q.; Liu, Z.; Yang, K.; Xu, C.; et al. Biome Responses to a Hydroclimatic Crisis in an Early Cretaceous (Barremian–Aptian) Subtropical Inland Lake Ecosystem, Northwest China. *Palaeogeogr. Palaeoclimatol. Palaeoecol.* **2023**, *622*, 111596. [CrossRef]
34. Jewuła, K.; Środoń, J.; Kuligiewicz, A.; Mikołajczak, M.; Liivamägi, S. Critical Evaluation of Geochemical Indices of Palaeosalinity Involving Boron. *Geochim. Cosmochim. Acta* **2022**, *322*, 1–23. [CrossRef]
35. Walker, C.T. Evaluation of Boron as a Paleosalinity Indicator and Its Application to Offshore Prospects. *Am. Assoc. Pet. Geol. Bull.* **1968**, *52*, 751–766. [CrossRef]
36. Wei, W.; Algeo, T.J. Elemental Proxies for Paleosalinity Analysis of Ancient Shales and Mudrocks. *Geochim. Cosmochim. Acta* **2020**, *287*, 341–366. [CrossRef]
37. Wang, A.; Wang, Z.; Liu, J.; Xu, N.; Li, H. The Sr/Ba Ratio Response to Salinity in Clastic Sediments of the Yangtze River Delta. *Chem. Geol.* **2021**, *559*, 119923. [CrossRef]
38. Lyons, P.C.; Palmer, C.A.; Bostick, N.H.; Fletcher, J.D.; Dulong, F.T.; Brown, F.W.; Brown, Z.A.; Krasnow, M.R.; Romankiw, L.A. Chemistry and Origin of Minor and Trace Elements in Vitrinite Concentrates from a Rank Series from the Eastern United States, England, and Australia. *Int. J. Coal Geol.* **1989**, *13*, 481–527. [CrossRef]
39. Eskenazy, G.; Delibaltova, D.; Mincheva, E. Geochemistry of Boron in Bulgarian Coals. *Int. J. Coal Geol.* **1994**, *25*, 93–110. [CrossRef]
40. Ye, C.; Yang, Y.; Fang, X.; Zhang, W.; Song, C.; Yang, R. Paleolake Salinity Evolution in the Qaidam Basin (NE Tibetan Plateau) between ~42 and 29 Ma: Links to Global Cooling and Paratethys Sea Incursions. *Sediment. Geol.* **2020**, *409*, 105778. [CrossRef]
41. Campbell, F.A.; Williams, G.D. Chemical Composition of Shales of Mannville Group (Lower Cretaceous) of Central Alberta, Canada. *Am. Assoc. Pet. Geol. Bull.* **1965**, *49*, 81–87. [CrossRef]
42. Chen, Z.; Chen, Z.; Zhang, W. Quaternary Stratigraphy and Trace-Element Indices of the Yangtze Delta, Eastern China, with Special Reference to Marine Transgressions. *Quat. Res.* **1997**, *47*, 181–191. [CrossRef]
43. Degens, E.T.; Williams, E.G.; Keith, M.L. Environmental Studies of Carboniferous Sediments Part I: Geochemical Criteria for Differentiating Marine from Fresh-Water Shales. *Am. Assoc. Pet. Geol. Bull.* **1957**, *41*, 2427–2455. [CrossRef]
44. Tao, S.; Xu, Y.; Tang, D.; Xu, H.; Li, S.; Chen, S.; Liu, W.; Cui, Y.; Gou, M. Geochemistry of the Shitoumei Oil Shale in the Santanghu Basin, Northwest China: Implications for Paleoclimate Conditions, Weathering, Provenance and Tectonic Setting. *Int. J. Coal Geol.* **2017**, *184*, 42–56. [CrossRef]
45. Deng, T.; Li, Y.; Wang, Z.; Yu, Q.; Dong, S.; Yan, L.; Hu, W.; Chen, B. Geochemical Characteristics and Organic Matter Enrichment Mechanism of Black Shale in the Upper Triassic Xujiahe Formation in the Sichuan Basin: Implications for Paleoweathering, Provenance and Tectonic Setting. *Mar. Pet. Geol.* **2019**, *109*, 698–716. [CrossRef]
46. Roy, D.K.; Roser, B.P. Climatic Control on the Composition of Carboniferous–Permian Gondwana Sediments, Khalaspir Basin, Bangladesh. *Gondwana Res.* **2013**, *23*, 1163–1171. [CrossRef]
47. Ganai, J.A.; Rashid, S.A. Anoxia and Fluctuating Climate Recorded from the Devonian–Carboniferous Black Shales, Tethys Himalaya, India: A Multi-Proxy Approach. *Int. J. Earth Sci.* **2019**, *108*, 863–883. [CrossRef]
48. Scheffler, K.; Buehmann, D.; Schwark, L. Analysis of Late Palaeozoic Glacial to Postglacial Sedimentary Successions in South Africa by Geochemical Proxies—Response to Climate Evolution and Sedimentary Environment. *Palaeogeogr. Palaeoclimatol. Palaeoecol.* **2006**, *240*, 184–203. [CrossRef]
49. Algeo, T.J.; Schwark, L.; Hower, J.C. High-Resolution Geochemistry and Sequence Stratigraphy of the Hushpuckney Shale (Swope Formation, Eastern Kansas): Implications for Climato-Environmental Dynamics of the Late Pennsylvanian Midcontinent Seaway. *Chem. Geol.* **2004**, *206*, 259–288. [CrossRef]
50. Doner, Z.; Kumral, M.; Demirel, I.H.; Hu, Q. Geochemical Characteristics of the Silurian Shales from the Central Taurides, Southern Turkey: Organic Matter Accumulation, Preservation and Depositional Environment Modeling. *Mar. Pet. Geol.* **2019**, *102*, 155–175. [CrossRef]
51. He, Y.; Zhu, X.; Qiu, Y.; Pang, L.; Zhao, T. Extreme Climate Changes Influenced Early Life Evolution at ~1.4 Ga: Implications from Shales of the Xiamaling Formation, Northern North China Craton. *Precambrian Res.* **2022**, *383*, 106901. [CrossRef]
52. Zeng, S.; Wang, J.; Zeng, Y.; Song, C.; Wang, D.; Zhan, W.; Sun, W. Episodic Volcanic Eruption and Arid Climate during the Triassic-Jurassic Transition in the Qiangtang Basin, Eastern Tethys: A Possible Linkage with the End-Triassic Biotic Crises. *J. Asian Earth Sci.* **2022**, *237*, 105345. [CrossRef]
53. Cole-Dai, J. Volcanoes and Climate. *WIREs Clim. Chang.* **2010**, *1*, 824–839. [CrossRef]
54. Timmreck, C. Modeling the Climatic Effects of Large Explosive Volcanic Eruptions. *WIREs Clim. Chang.* **2012**, *3*, 545–564. [CrossRef]
55. Chen, X.; Jin, X.; Zhu, X.; Zhong, N.; Zhang, Z. Origins of Organic Matter, Paleoenvironment, and Hydrocarbon Potential of the Carboniferous Source Rocks from Shibei Sag, Junggar Basin, NW China. *ACS Earth Sp. Chem.* **2023**, *7*, 92–109. [CrossRef]
56. Zhang, K.; Jin, W.; Lin, H.; Dong, C.; Wu, S. Major and Trace Elemental Compositions of the Upper Carboniferous Batamayineishan Mudrocks, Wulungu Area, Junggar Basin, China: Implications for Controls on the Formation of the Organic-Rich Source Rocks. *Mar. Pet. Geol.* **2018**, *91*, 550–561. [CrossRef]

57. Bennett, W.W.; Canfield, D.E. Redox-Sensitive Trace Metals as Paleoredox Proxies: A Review and Analysis of Data from Modern Sediments. *Earth-Sci. Rev.* **2020**, *204*, 103175. [CrossRef]
58. Algeo, T.J.; Li, C. Redox Classification and Calibration of Redox Thresholds in Sedimentary Systems. *Geochim. Cosmochim. Acta* **2020**, *287*, 8–26. [CrossRef]
59. Rimmer, S.M. Geochemical Paleoredox Indicators in Devonian–Mississippian Black Shales, Central Appalachian Basin (USA). *Chem. Geol.* **2004**, *206*, 373–391. [CrossRef]
60. Jones, B.; Manning, D.A.C. Comparison of Geochemical Indices Used for the Interpretation of Palaeoredox Conditions in Ancient Mudstones. *Chem. Geol.* **1994**, *111*, 111–129. [CrossRef]
61. Ossa, F.O.; Bekker, A.; Hofmann, A.; Poulton, S.W.; Ballouard, C.; Schoenberg, R. Limited Expression of the Paleoproterozoic Oklo Natural Nuclear Reactor Phenomenon in the Aftermath of a Widespread Deoxygenation Event ~2.11–2.06 Billion Years Ago. *Chem. Geol.* **2021**, *578*, 120315. [CrossRef]
62. Zhu, B.; Yang, T.; Wang, J.; Chen, X.; Pan, W.; Chen, Y. Multiple Controls on the Paleoenvironment of the Early Cambrian Black Shale-Chert in the Northwest Tarim Basin, NW China: Trace Element, Iron Speciation and Mo Isotopic Evidence. *Mar. Pet. Geol.* **2022**, *136*, 105434. [CrossRef]
63. Tribovillard, N.; Algeo, T.J.; Lyons, T.; Riboulleau, A. Trace Metals as Paleoredox and Paleoproductivity Proxies: An Update. *Chem. Geol.* **2006**, *232*, 12–32. [CrossRef]
64. Fathy, D.; Wagreich, M.; Fathi, E.; Ahmed, M.S.; Leila, M.; Sami, M. Maastrichtian Anoxia and Its Influence on Organic Matter and Trace Metal Patterns in the Southern Tethys Realm of Egypt during Greenhouse Variability. *ACS Omega* **2023**, *8*, 19603–19612. [CrossRef] [PubMed]
65. Pan, Y.; Huang, Z.; Guo, X.; Wang, R.; Lash, G.G.; Fan, T.; Liu, W. A Re-Assessment and Calibration of Redox Thresholds in the Permian Lucaogou Formation of the Malang Sag, Santanghu Basin, Northwest China. *Mar. Pet. Geol.* **2022**, *135*, 105406. [CrossRef]
66. Zhang, Y.; Hu, S.; Shen, C.; Liao, Z.; Xu, J.; Zhang, X. Factors Influencing the Evolution of Shale Pores in Enclosed and Semi-Enclosed Thermal Simulation Experiments, Permian Lucaogou Formation, Santanghu Basin, China. *Mar. Pet. Geol.* **2022**, *135*, 105421. [CrossRef]
67. Liu, B.; Song, Y.; Zhu, K.; Su, P.; Ye, X.; Zhao, W. Mineralogy and Element Geochemistry of Salinized Lacustrine Organic-Rich Shale in the Middle Permian Santanghu Basin: Implications for Paleoenvironment, Provenance, Tectonic Setting and Shale Oil Potential. *Mar. Pet. Geol.* **2020**, *120*, 104569. [CrossRef]
68. Jiao, X.; Liu, Y.; Yang, W.; Zhou, D.; Wang, S.; Jin, M.; Sun, B.; Fan, T. Mixed Biogenic and Hydrothermal Quartz in Permian Lacustrine Shale of Santanghu Basin, NW China: Implications for Penecontemporaneous Transformation of Silica Minerals. *Int. J. Earth Sci.* **2018**, *107*, 1989–2009. [CrossRef]
69. Hong, S.K.; Shinn, Y.J.; Choi, J.; Lee, H.S. Estimation of Original Kerogen Type and Hydrogen Index Using Inorganic Geochemical Proxies: Implications for Assessing Shale Gas Potential in the Devonian Horn River Formation of Western Canada. *Am. Assoc. Pet. Geol. Bull.* **2018**, *102*, 2075–2099. [CrossRef]
70. Cardott, B.J. Thermal Maturity of Woodford Shale Gas and Oil Plays, Oklahoma, USA. *Int. J. Coal Geol.* **2012**, *103*, 109–119. [CrossRef]
71. Hazra, B.; Singh, D.P.; Chakraborty, P.; Singh, P.K.; Sahu, S.G.; Adak, A.K. Using Rock-Eval S4Tpeak as Thermal Maturity Proxy for Shales. *Mar. Pet. Geol.* **2021**, *127*, 104977. [CrossRef]
72. Katz, B.J.; Lin, F. Consideration of the Limitations of Thermal Maturity with Respect to Vitrinite Reflectance, Tmax, and Other Proxies. *Am. Assoc. Pet. Geol. Bull.* **2021**, *105*, 695–720. [CrossRef]
73. Yang, S.; Horsfield, B. Critical Review of the Uncertainty of Tmax in Revealing the Thermal Maturity of Organic Matter in Sedimentary Rocks. *Int. J. Coal Geol.* **2020**, *225*, 103500. [CrossRef]
74. Dang, W.; Nie, H.; Zhang, J.; Tang, X.; Jiang, S.; Wei, X.; Liu, Y.; Wang, F.; Li, P.; Chen, Z. Pore-Scale Mechanisms and Characterization of Light Oil Storage in Shale Nanopores: New Method and Insights. *Geosci. Front.* **2022**, *13*, 101424. [CrossRef]
75. Huang, H.; Li, R.; Chen, W.; Chen, L.; Jiang, Z.; Xiong, F.; Guan, W.; Zhang, S.; Tian, B. Revisiting Movable Fluid Space in Tight Fine-Grained Reservoirs: A Case Study from Shahejie Shale in the Bohai Bay Basin, NE China. *J. Pet. Sci. Eng.* **2021**, *207*, 109170. [CrossRef]
76. Lu, S.; Huang, W.; Chen, F.; Li, J.; Wang, M.; Xue, H.; Wang, W.; Cai, X. Classification and Evaluation Criteria of Shale Oil and Gas Resources: Discussion and Application. *Pet. Explor. Dev.* **2012**, *39*, 268–276. [CrossRef]
77. Neuzil, C.E. Permeability of Clays and Shales. *Annu. Rev. Earth Planet. Sci.* **2019**, *47*, 247–273. [CrossRef]
78. Mustafa, A.; Tariq, Z.; Mahmoud, M.; Radwan, A.E.; Abdulraheem, A.; Abouelresh, M.O. Data-Driven Machine Learning Approach to Predict Mineralogy of Organic-Rich Shales: An Example from Qusaiba Shale, Rub' Al Khali Basin, Saudi Arabia. *Mar. Pet. Geol.* **2022**, *137*, 105495. [CrossRef]
79. Jarvie, D.M.; Hill, R.J.; Ruble, T.E.; Pollastro, R.M. Unconventional Shale-Gas Systems: The Mississippian Barnett Shale of North-Central Texas as One Model for Thermogenic Shale-Gas Assessment. *Am. Assoc. Pet. Geol. Bull.* **2007**, *91*, 475–499. [CrossRef]

80. Li, H. Research Progress on Evaluation Methods and Factors Influencing Shale Brittleness: A Review. *Energy Rep.* **2022**, *8*, 4344–4358. [CrossRef]
81. Ye, Y.; Tang, S.; Xi, Z. Brittleness Evaluation in Shale Gas Reservoirs and Its Influence on Fracability. *Energies* **2020**, *13*, 388. [CrossRef]